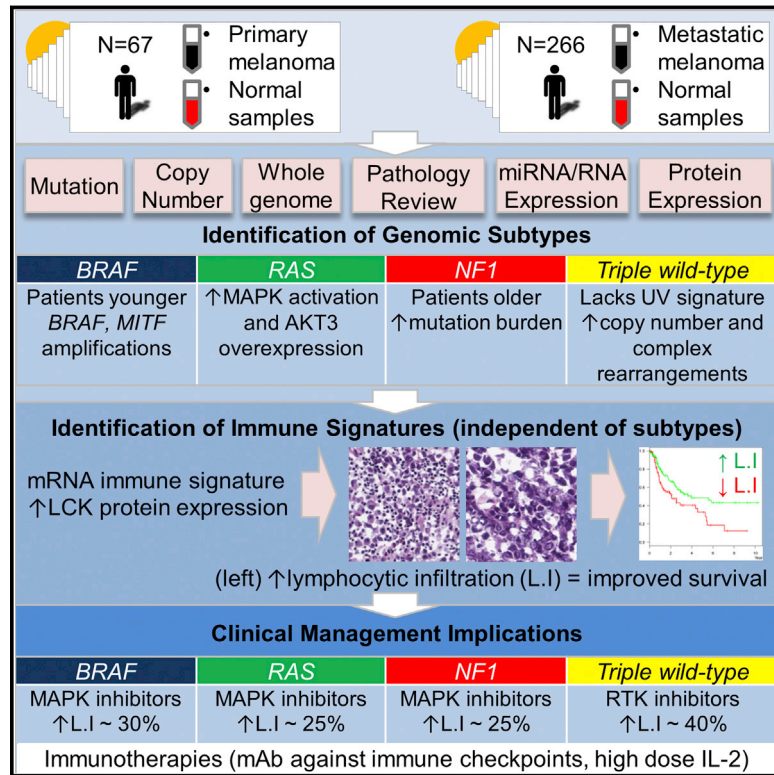# Genomic Classification of Cutaneous Melanoma

Graphical Abstract

Authors

The Cancer Genome Atlas Network

Correspondence

irwatson@mdanderson.org (I.R.W.),
jgershen@mdanderson.org (J.E.G.),
lchin@mdanderson.org (L.C.)

In Brief

An integrative analysis of cutaneous melanomas establishes a framework for genomic classification into four subtypes that can guide clinical decision-making for targeted therapies. A subset of each of the genomic classes expresses considerable immune infiltration markers that are associated with improved survival, with potential implications for immunotherapy.

Highlights

- Represents the largest integrative analysis of cutaneous melanoma (331 patients)

- Establishes a framework for melanoma genomic classification: *BRAF*, *RAS*, *NF1*, and Triple-WT

- Identifies additional subtypes that may benefit from MAPK- and RTK-targeted therapies

- Multi-dimensional analyses identify immune signatures associated with improved survival

Genomic Classification of Cutaneous Melanoma

The Cancer Genome Atlas Network[1,*,*,*]
[1]Cancer Genome Atlas Program Office, National Cancer Institute at NIH, 31 Center Drive, Bldg. 31, Suite 3A20, Bethesda, MD 20892, USA
*Correspondence: irwatson@mdanderson.org (I.R.W.), jgershen@mdanderson.org (J.E.G.), lchin@mdanderson.org (L.C.)
http://dx.doi.org/10.1016/j.cell.2015.05.044

SUMMARY

We describe the landscape of genomic alterations in cutaneous melanomas through DNA, RNA, and protein-based analysis of 333 primary and/or metastatic melanomas from 331 patients. We establish a framework for genomic classification into one of four subtypes based on the pattern of the most prevalent significantly mutated genes: mutant *BRAF*, mutant *RAS*, mutant *NF1*, and Triple-WT (wild-type). Integrative analysis reveals enrichment of *KIT* mutations and focal amplifications and complex structural rearrangements as a feature of the Triple-WT subtype. We found no significant outcome correlation with genomic classification, but samples assigned a transcriptomic subclass enriched for immune gene expression associated with lymphocyte infiltrate on pathology review and high LCK protein expression, a T cell marker, were associated with improved patient survival. This clinicopathological and multidimensional analysis suggests that the prognosis of melanoma patients with regional metastases is influenced by tumor stroma immunobiology, offering insights to further personalize therapeutic decision-making.

INTRODUCTION

Diagnosis and surgical resection of early-stage primary cutaneous melanoma is often curative for patients with localized disease, but the prognosis is less favorable for patients with regional metastases. Using the technique of lymphatic mapping and sentinel lymph node (SLN) biopsy (Gershenwald and Ross, 2011), early surgical intervention for patients with microscopic regional lymph node metastases (i.e., positive SLNs) has recently been found useful for prognosis, may improve survival in a subgroup of such patients, and serves to guide the use of adjuvant therapy (Morton et al., 2014). Overall, survival has historically been poor for patients with distant metastatic disease, and response to conventional chemotherapy has been infrequent (Balch et al., 2009).

Hot-spot mutations in the V600 codon of *BRAF* (35%–50% of melanomas) and Q61 codons (less frequently, the G12 or G13 codon) of *NRAS* (10%–25%) led to the development of highly selective kinase inhibitors that target the MAPK pathway (Tsao et al., 2012). Recent clinical trials have provided proof of principle that therapeutic agents targeting activating mutations for patients with unresectable disease and/or distant melanoma metastases can be identified through genetic analyses. The Food and Drug Administration (FDA) has approved three such inhibitors: vemurafenib, dabrafenib, and trametinib (McArthur and Ribas, 2013). Although antitumor responses have been dramatic, they have rarely been durable. Additional targets and combinatorial treatment strategies are clearly needed.

Recent studies using next-generation sequencing (NGS) have identified additional genetic aberrations (Berger et al., 2012; Hodis et al., 2012; Krauthammer et al., 2012) that provide insights into the biological heterogeneity of melanoma and also have potentially important implications for prognosis and therapy. However, previous biomarker studies in melanoma have either focused on single high-throughput platforms of large sample sets (Hodis et al., 2012; Krauthammer et al., 2012; Winnepenninckx et al., 2006) or multi-platform analyses of fewer samples (Mann et al., 2013; Rakosy et al., 2013). No prior study has integrated multi-platform data from such a large cohort of clinicopathologically well-annotated samples.

To address this gap, The Cancer Genome Atlas (TCGA) program performed a systematic multi-platform characterization of 333 cutaneous melanomas at the DNA, RNA, and protein levels to create a catalog of somatic alterations and describe their potential biological and clinical significance. We established a genomic/transcriptomic framework of classification that has potential implications for prognosis and therapy and that may relate to recent advances in immunotherapy.

RESULTS

Multi-dimensional Genomic Characterization of Cutaneous Melanoma

Compared to most solid tumors, primary melanomas are generally small at diagnosis; and in routine clinical practice, most or all of primary tumor tissue is used for diagnostic evaluation and is not available for molecular analyses. Accordingly, our study included samples from thick primaries, regional, and distant metastatic sites.

We collected frozen tumor samples from 333 cutaneous primary and/or metastatic melanomas with matched peripheral blood from 331 adult patients from 14 tissue source sites under protocols approved by the relevant Institutional Review Boards. Clinicopathological characteristics are summarized in Table S1A. The samples consisted of 67 (20%) primary cutaneous melanomas (all originating from non-glabrous skin) and 266 (80%) metastases. Of the metastases, 212 were from regional sites (160 from regional lymph nodes and 52 from regional skin/soft tissue), and 35 were from distant sites (Table S1A–S1C). At initial

diagnosis, patients had primary tumors (whether or not the primary tumors were included in the TCGA molecular analyses) that were thicker (median and mean, 2.7 mm and 4.9 mm, respectively) than in population-based registry data (Baade et al., 2012; Criscione and Weinstock, 2010). Matched primary and metastatic samples were available for complete molecular analyses from only two patients.

We performed six types of global molecular analysis: solution-based hybrid-capture whole-exome sequencing (WES, n = 320 samples), DNA copy-number profiling by Affymetrix SNP 6.0 arrays (n = 333), mRNA sequencing (n = 331), microRNA sequencing (n = 323), DNA methylation profiling (n = 333), and reverse-phase protein array (RPPA) expression profiling (n = 202). Complete data for all six platforms were available for a core set of 199 samples. *TERT* promoter mutations at C228T and C250T were assessed by PCR-Sanger sequencing in a subset of 115 samples. Deep-coverage whole-genome sequencing and low-pass whole-genome sequencing were performed on subsets of 38 samples and 119 samples, respectively. Clinicopathological and molecular data associated with each patient are presented in a patient-centric table (Table S1D); complete methods and results of the analyses are described in the Supplemental Experimental Procedures. The standard data package associated with this report (frozen on November 14, 2013) is available at the GDAC Firehose (http://gdac.broadinstitute.org/runs/stddata__2013_11_14/data/SKCM/20131114) and at Data Portal (https://tcga-data.nci.nih.gov/docs/publications/skcm_2015/).

Identification of Significantly Mutated Genes

WES was performed on paired tumor and germline normal genomic DNA from 318 patients, including primary (n = 58) and metastatic (n = 262) melanomas with a mean exon coverage of 87×, adequate for detecting a single-nucleotide variant (SNV) at an allelic fraction of 0.3 with a power of 80% (Carter et al., 2012) (see Supplemental Experimental Procedures). In total, we identified 228,987 mutations, including both SNVs and indels. Targeted validation of 455 SNVs observed in the significantly mutated genes (see below) in a subset of tumor DNAs (n = 277) revealed an overall validation rate of 96% (see Supplemental Experimental Procedures). The mean mutation rate was 16.8 mutations/Mb, the highest reported for any cancer type thus far analyzed by TCGA (Lawrence et al., 2013) (Figure S1A) and corroborates findings from other NGS melanoma studies (e.g., Hodis et al., 2012) and other ultraviolet (UV)-driven skin cancers such as basal and squamous cell carcinomas (e.g., Jayaraman et al., 2014). Consistent with UV radiation's mutagenic role in melanoma, most samples showed a high fraction of C>T transitions at dipyrimidines (median 77.7%; interquartile range 69.4%–82.6%) and CC>TT mutations (median 3.9%; interquartile range 2.0%–5.7%) (Figure S1A). We classified samples in which C>T transitions at dipyrimidine sites accounted for more than 60% or CC>TT mutations more than 5% of the total mutation burden as possessing a UV signature (Brash, 2015): 44 (76%) of the 58 primary and 221 (84%) of the 262 metastatic samples had such a signature.

Given the statistical challenge of defining significance against a high background mutation rate, we used two algorithms to define significantly mutated genes (SMGs): MutSig and InVEx (Hodis et al., 2012; Lawrence et al., 2014; Lawrence et al., 2013). MutSig takes into consideration patient-specific mutation frequencies and spectra, mRNA expression levels, and gene-specific DNA replication times; InVEx controls for patient-specific, gene-specific, and nucleotide-context-specific mutation probabilities (see Supplemental Experimental Procedures). WES analysis by InVEx identified 13 SMGs (Bonferroni p < 0.05, or 20 SMGs at Q < 0.1) by either functional mutation burden or loss-of-function tests, all of them among the 42 SMGs identified by MutSig (Q < 0.1) (Tables S2A–S2D and Figure S1B). The 13 SMGs included previously described melanoma oncogenes and tumor suppressors (*BRAF*, *NRAS*, *CDKN2A*, *TP53*, and *PTEN*), as well as recently identified mutated genes (*RAC1*, *MAP2K1*, *PPP6C*, and *ARID2*) (Hodis et al., 2012; Krauthammer et al., 2012; Nikolaev et al., 2012). Our cohort also had sufficient statistical power to annotate several previously implicated melanoma genes as SMGs (*NF1*, *IDH1*, and *RB1*) (Andersen et al., 1993; Draper et al., 1986; Lopez et al., 2010). We also identified *DDX3X*, a putative RNA helicase, as a novel candidate melanoma SMG (Figures 1A and S1C). SMGs with UV-induced hot-spot mutations included *RAC1* (6.9%) and *IDH1* (6.2%) (Figure S1C). The *RAC1* hot-spot mutation has been linked to resistance to BRAF inhibitors (Van Allen et al., 2014; Watson et al., 2014). Similar to findings in other tumor types, *IDH1*-mutated samples were enriched in the high CpG island methylator phenotype (CIMP) subgroup (Figures S1D–S1G) (Noushmehr et al., 2010).

Additionally, two genes (*MRPS31* and *RPS27*) that encode ribosomal proteins were identified by MutSig as SMGs. Both possess presumptive UV-induced hot-spot mutations in their 5′ UTR (in ~5% and ~9% of samples, respectively) (Figure S1H). *MRPS31* encodes a mitochondrial ribosomal protein not previously associated with cancer; RPS27 is a component of the 40S ribosomal subunit whose overexpression has been reported in melanoma (Santa Cruz et al., 1997). The recurrent mutation in *RPS27* was recently shown to expand the 5′ TOP element, a motif known to control mRNA translation regulated through the PI(3)K/AKT and mTOR pathways (Dutton-Regester et al., 2014).

Genomic Classification of Melanoma

One of the most significant successes in clinical practice has been the development of targeted therapies for patients with activating driver mutations (McArthur and Ribas, 2013; Tsao et al., 2012). We therefore classified melanomas based on identified SMGs and their distribution in our cohort (n = 318 cases with WES data; described below, Figure 1A, and Table 1) to create a framework that could be used for personalized therapeutic decisions.

BRAF Subtype

The largest genomic subtype is defined by the presence of *BRAF* hot-spot mutations. Of the 318, 52% (n = 166) harbored *BRAF* somatic mutations. Of those, 145 targeted the well-documented V600 amino acid residue: V600E (n = 124), V600K (n = 18), and V600R (n = 3). The second most frequent *BRAF* mutation targeted the K601 residue (n = 5). As in previous reports (Pollock et al., 2003), both *BRAF* V600 and K601
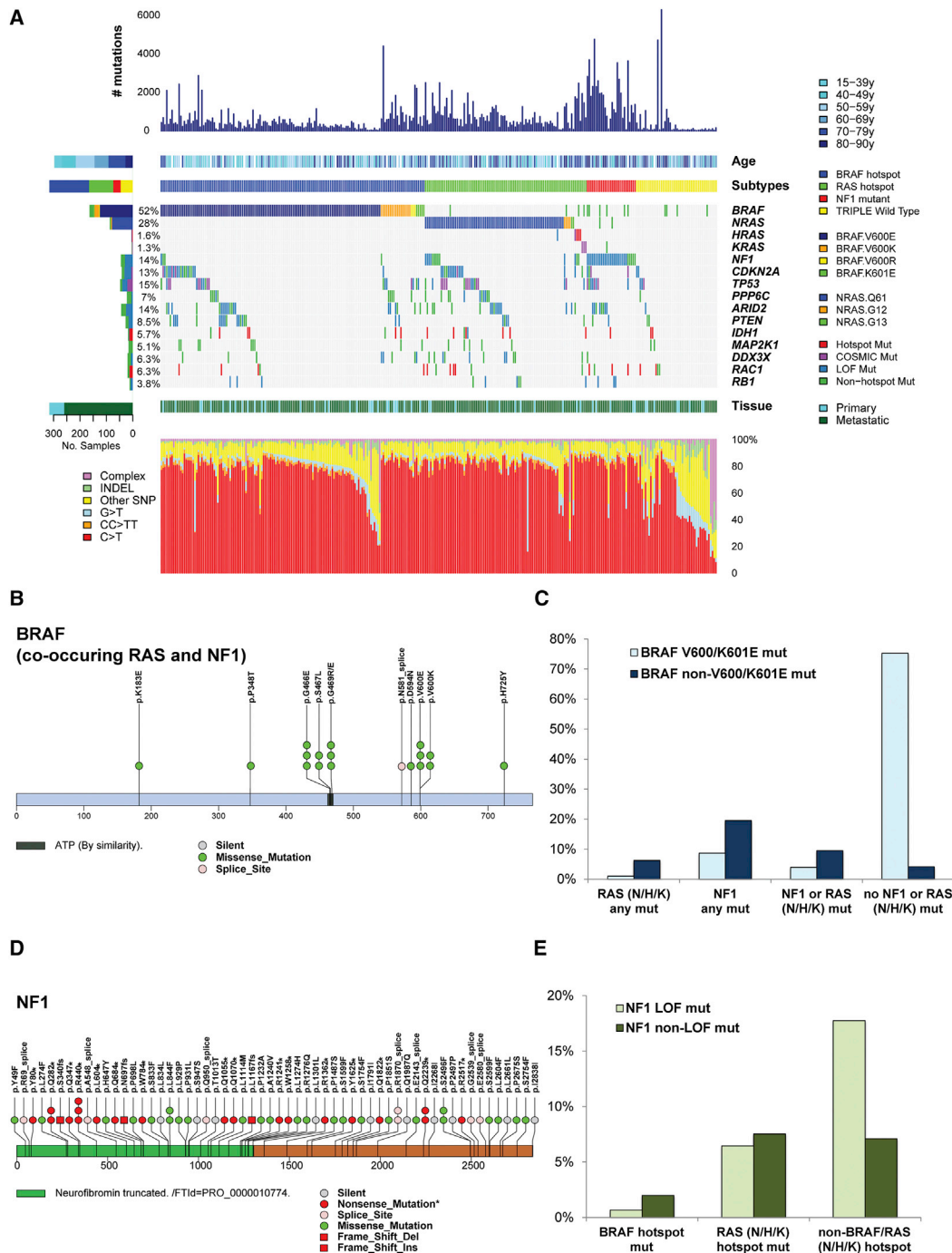
Figure 1. Landscape of Driver Mutations in Melanoma

(A) Total number of mutations, age at melanoma accession, and mutation subtype (*BRAF*, *RAS* [*N/H/K*], *NF1*, and Triple-WT) are indicated for each sample (top). (Not shown are one hyper-mutated and one co-occurring *NRAS BRAF* hot-spot mutant). Color-coded matrix of individual mutations (specific *BRAF* and *NRAS* mutations indicated) (middle), type of melanoma specimen (primary or metastasis), and mutation spectra for all samples (bottom) are indicated. For the two samples with both a matched primary and metastatic sample, only the mutation information from the metastasis was included.

(B) *BRAF* mutations that co-occur with *RAS* family member and *NF1* mutations are illustrated across the BRAF protein.

(C) Fraction of *BRAF* V600/K601E and non-V600/K601E co-occurring with the *RAS (N/H/K)*, *NF1*, *NF1/RAS (N/H/K)* combined cohort and no *NF1/RAS (N/H/K)* mutations.

(D) *NF1* mutations found in melanoma whole-exome sequencing data across the NF1 protein.

(E) Fraction of *NF1* missense and truncating mutations co-occurring with *RAS* hot-spot or non-*BRAF/RAS* hot-spot mutations. (Mut, mutation).

See also Figure S1.

Table 1. Implications for Clinical Management Based on Features Identified by Comprehensive Molecular TCGA Analysis

Mutation Subtypes	BRAF	RAS	NF1	Triple Wild-Type
[1]MAPK pathway	[1]BRAF V600, K601	[1](N/H/K) RAS G12, G13, Q61	[1]NF1 LoF mut; (BRAF non-hot-spot mut)	[1]KIT COSMIC mut/amp, PDGFRa amp, KDR (VEGFR2) amp; rare COSMIC GNA11 mut, GNAQ mut
[2]Cell-cycle pathway	CDKN2A mut/del/h-meth (~60%); [2](CDK4 COSMIC mut)	CDKN2A mut/del/h-meth (~70%); CCND1 amp (~10%), [2](CDK4 COSMIC mut)	CDKN2A mut/del/h-meth (~70%); RB1 mut (~10%)	CDKN2A mut/del/h-meth (~40%); CCND1 amp (~10%), [2]CDK4 amp (15%)
[3]DNA damage response and cell death pathways	TP53 mut (~10%); [3](note: TP53 wild-type in ~90% of BRAF subtype)	TP53 mut (20%)	TP53 mut (~30%)	[3]MDM2 amp (~15%); [3]BCL2 upregulation
[4]PI3K/Akt pathway	[4]PTEN mut/del (~20%); [4](rare AKT1/3 and PIK3CA COSMIC mut)	[4]AKT3 overexpression (~40%); [4](rare AKT1/3 and PIK3CA COSMIC mut)	[4]AKT3 overexpression (~30%)	[4]AKT3 overexpression (~20%)
[5]Epigenetics	[5]IDH1 mut, [5](rare EZH2 COSMIC mut); [5]ARID2 mut (~15%)	[5]IDH1 mut, [5](rare EZH2 COSMIC mut); [5]ARID2 mut (~15%)	[5]IDH1 mut, [5](EZH2 mut); [5]ARID2 mut (~30%)	[5]IDH1 mut, [5](rare EZH2 COSMIC mut)
Telomerase pathway	Promoter mut (~75%)	Promoter mut (~70%)	Promoter mut (~85%)	Promoter mut (< 10%); TERT amp (~15%)
Other pathways	PD-L1 amp, MITF amp, PPP6C mut (~10%)	PPP6C mut (~15%)		
[6]High immune infiltration (pathology)	~30%	~25%	~25%	~40%
Class 1: Clinically actionable	[1]BRAF inhibitors; [1]MEK inhibitors	[1]MEK inhibitors		[1]C-KIT inhibitors (imatinib, dasatinib, nilotinib, sunitinib); PKC inhibitors (AEB071)
	[2]CDK inhibitors	[1,2]CDK inhibitors		[2]CDK inhibitors
	[3]MDM2/p53 interaction inhibitors			[3]MDM2/p53 interaction inhibitors
	[4]PI3K/Akt/mTOR inhibitors	[4]PI3K/Akt/mTOR inhibitors	[4]PI3K/Akt/mTOR inhibitors	[4]PI3K/Akt/mTOR inhibitors
	[6]immunotherapies (mAb against immune checkpoint proteins, high dose bolus IL-2, interferon-α2b)			
Class 2: Translationally actionable	[1]ERK inhibitors	[1]ERK inhibitors	[1]MEK inhibitors; [1]ERK inhibitors	
	[5]IDH1 inhibitors	[5]IDH1 inhibitors	[5]IDH1 inhibitors	[5]IDH1 inhibitors
	[5]EZH2 inhibitors	[5]EZH2 inhibitors	[5]EZH2 inhibitors	[5]EZH2 inhibitors
	(PPP6C) Aurora kinase inhibitors	(PPP6C) Aurora kinase inhibitors		
Class 3: Pre-clinical	[5]ARID2 chromatin remodelers (synthetic lethality)	[5]ARID2 chromatin remodelers (synthetic lethality)	[5]ARID2 chromatin remodelers (synthetic lethality)	[3](BCL2) BH3 mimemitcs

Prominent mechanisms of pathway alterations in BRAF, RAS, NF1 and Triple Wild-Type (WT) subtypes with potential predictive genetic alterations indicated ([1], [2], [3], [4], [5], [6]) for Class 1 (clinically actionable alterations), Class 2 (translationally actionable that still require additional data [evidence] to support use in point-of-care decision making), and Class 3 (pre-clinical evidence has demonstrated biological importance but has not yet demonstrated clinical relevance) biomarkers. High immune infiltration (pathology) is percentage of samples in respective mutation subtype with LScores of 5–6. Amp, amplification; del, deletion; mut, mutation, h-meth, hypermethylation.

hot-spot mutations were anti-correlated with hot-spot NRAS mutations (Fisher's exact p < 1e−15). In contrast, BRAF non-hot-spot mutations (including eight exon 11 mutations) co-occurred with RAS (N/H/K) hot-spot and NF1 mutations (Figures 1B and 1C).

RAS Subtype

The second major subtype is defined by the presence of RAS hot-spot mutations, including known amino acid changes with functional consequences, in all three RAS family members (N-, K- and H-RAS). Overall, 28% (n = 88) had NRAS somatic

mutations. Of those, 86 had hot-spot mutations, including Q61R (n = 35), Q61K (n = 28), Q61L (n = 11), Q61H (n = 4), 61_62QE > HK (n = 1), G12R/D/A (n = 4), and G13R/D (n = 3). We also identified less-frequent mutations in other *RAS* family members, including four hot-spot *HRAS* (G13D, G13S, and Q61K [n = 2]) and three *KRAS* (G12D, G12R, and Q61R) mutations; all were mutually exclusive with *NRAS* and *BRAF* V600 and K601 mutations.

NF1 Subtype

The third most frequently observed SMG in the MAPK pathway was *NF1*, which was mutated in 14% of samples. More than half of its mutations were predicted to be loss-of-function (LoF) events, including 27 nonsense, 9 splice-site, and 4 frame-shift indels out of 65 mutations (InVEx LoF analysis: p = 1.8e−11, Q = 9.1e−12) (Figures 1D and 1E). *NF1* subtype (n = 28) had the highest mutation prevalence (39 mutations/Mb, more than double that of the other three subtypes). Since NF1 is a GTPase-activating protein known to downregulate RAS activity through its intrinsic GTPase activity, LoF mutation of *NF1* can be viewed as an alternative way to activate the canonical MAPK signaling pathway. Indeed, in this cohort, *NF1* was mutated in 38.7% of non-hot-spot *BRAF/NRAS* melanomas (29/75) and in ~70% of non-hot-spot *BRAF/NRAS* samples with a UV-signature (26/38) (Figure 1A). Furthermore, *NF1* mutations were anti-correlated with hot-spot *BRAF* mutations (p = 1.9e−9), but not hot-spot *RAS* mutations (Figure 1A).

Triple Wild-Type Subtype

We defined the Triple-WT subtype (n = 46) as a heterogeneous subgroup characterized by a lack of hot-spot *BRAF, N/H/K-RAS*, or *NF1* mutations. This lack of hot-spot mutations was not due to lower tumor purity or ploidy, since power calculation taking into account sample-specific purity and ploidy (Carter et al., 2012) showed that our sequencing coverage is powered to detect sub-clonal mutations at a 6% allelic fraction on average in Triple-WT subtype (see Supplemental Experimental Procedures). To identify rare low-frequency driver mutations in this subtype, we cross-referenced all observed SNVs to recurrently mutated base pairs (n > 20) in the COSMIC database v60 and identified 11 additional genes with recurrent COSMIC mutations (Table S2E). Several COSMIC mutations, including known drivers of uveal melanoma—*GNAQ* (n = 1) and *GNA11* (n = 2), *KIT* (n = 6), as well as *CTNNB1* (n = 3) and *EZH2* (n = 1)—were found in the Triple-WT subtype.

Molecular Characteristics of the Four Genomic Subtypes

Clinically, patients in the *BRAF* subtype were younger than patients in the other subtypes, while those in the *NF1* subtype were significantly older (rank sum p = 0.008). Regardless of subtype, patients with *TP53* mutant melanomas had significantly higher mutation counts and number of C>T transitions (rank sum p = 1.35 e−05 and p = 1.1 e−05, respectively). However, no significant difference was observed in post-accession survival (i.e., survival calculated from date of biospecimen collection/accession to date of last follow-up or death, see Supplemental Experimental Procedures). Therefore, we next explored the molecular heterogeneity among these genomic subtypes by integrative analyses.

UV Signature

We noted that only 30% (14/46) of samples in the Triple-WT subtype harbored a UV signature, compared to 90.7% of samples with a *BRAF* hot-spot mutation (136/150), 93.5% with a *RAS* (N-H-K) hot-spot mutation (86/92), and 92.9% of the *NF1* subtype (26/28) (Figure S1I) (Fisher's exact test p = 1e−15). In contrast, Triple-WT samples had more copy-number changes and complex structural arrangements compared to the other groups.

Somatic Copy-Number Alterations

We assessed the patterns of somatic copy-number alteration (CNA) across subtypes. Although global patterns of arm-level alterations were similar, the Triple-WT had significantly more copy-number segments (Figures S2A and S2B) and was enriched for focal amplifications targeting known oncogenes. For example, we found significant 4q12 focal amplification containing the oncogene *KIT* only in the Triple-WT cohort (Figure 2A). Two other adjacent oncogenes, *PDGFRA* and *KDR (*also known as *VEGFR2)*, were frequently co-amplified with *KIT* (Figure 2B). We also observed high-level focal CNAs containing the oncogenes *CDK4* and *CCND1* (p < 0.01, FDR < 0.05), consistent with previous studies (Curtin et al., 2005), as well as *MDM2* and *TERT* (p < 0.05, FDR < 0.05) to be significantly enriched in Triple-WT melanomas (Figures 2B and 2C). In contrast, focal amplifications of *BRAF*, the melanocyte lineage-specific oncogene *MITF* (p < 0.01, FDR < 0.05), and the ligand for the co-inhibitory immune checkpoint protein PD-1, PD-L1 gene (*CD274*), were observed at significant frequencies in the *BRAF* mutant subtype (Figures 2, S2C, and S2D), whereas *NRAS* amplifications co-occurred in tumors with *NRAS* mutations (Figure S2C). *CD274* amplifications (which encodes PD-L1) are particularly noteworthy given the potential clinical value of PD-L1 expression in predicting response to PD-1 pathway inhibitors (Tumeh et al., 2014).

Structural Rearrangements

To define fusion events, we performed an integrative analysis using copy-number (n = 333), RNA-seq (n = 331), and whole-genome sequencing (WGS) data complemented by low-pass (n = 119) and deep (n = 38) sequencing. In total, 224 candidate fusion drivers were identified (Table S3A). Although there was only one recurrent fusion (*GRM8-CNTNAP2,* n = 2), we discovered a number of melanoma-associated genes recurrently fused to various gene partners (Figure S2E), including *BRAF* (*ATG7-BRAF* and *TAX1BP1-BRAF*), *RAF1* (*TRAK1-RAF1, RAF1-AGGF1,* and *CLCN6-RAF1*), and *AKT3* (*CEP170-AKT3, AKT3-PLD5, ZEB2-AKT3,* and *ARHGAP30-AKT3*). We also identified three *MITF* fusions (*MITF-FOXP1, CADM2-MITF,* and *FRMD4B-MITF*) and three *HMGA2* fusions (*PCBP2-HMGA2, TSFM-HMGA2,* and *SENP1-HMGA2*). Eight of the 224 candidate driver fusions (*ATG7-BRAF, TAX1BP1-BRAF, LBH-FLT4, LCLAT1-EPHA3, TRAK1-RAF1, CLCN6-RAF1, CPSF4L-ERBB4,* and *MOBKL1B-EPHB1*) possessed a predicted intact kinase domain. Although additional functional studies are required to determine the role of these fusions in melanoma, unbiased pathway analyses of candidate fusions suggest biological functions relevant to melanoma (Tables S3B and S3C).

We saw significant enrichment for the 224 predicted fusion drivers in the Triple-WT subtype (p = 2e−04) (Figure S2F). Using
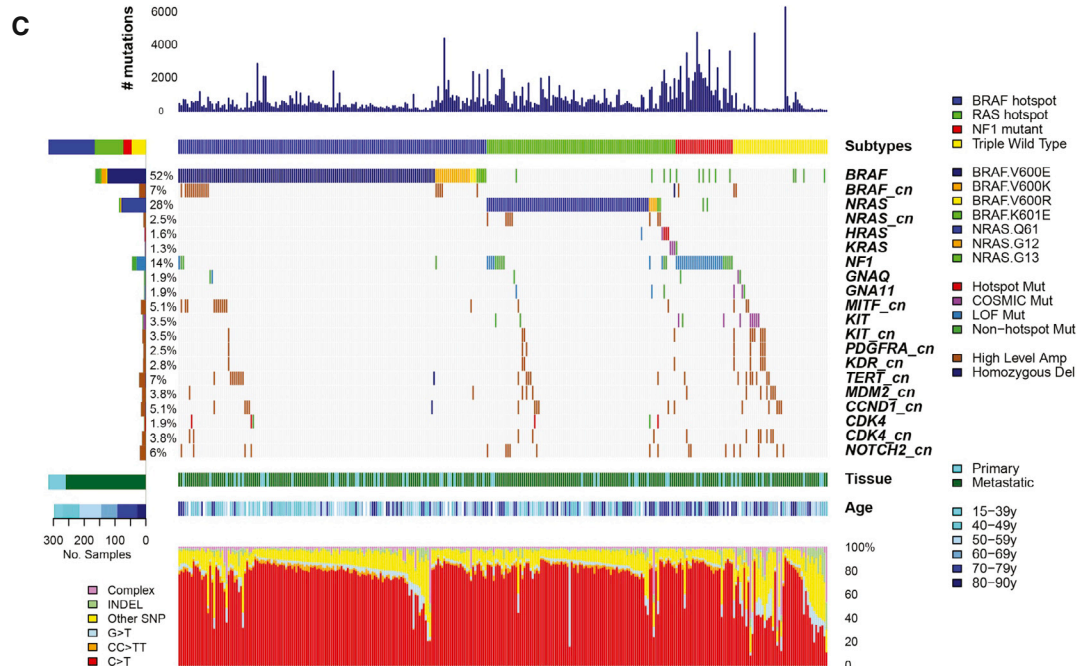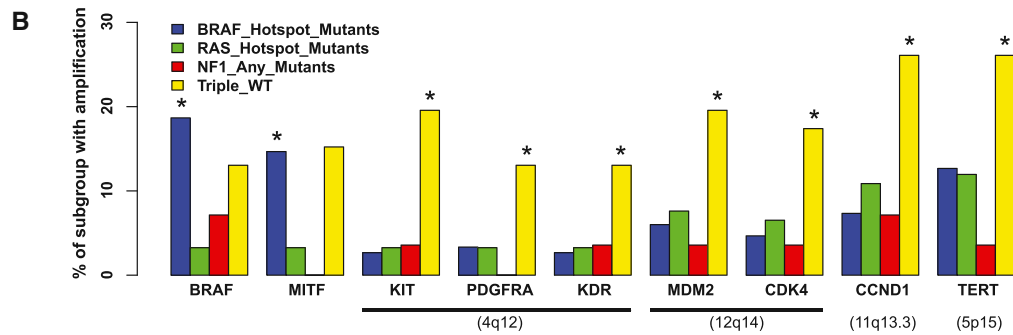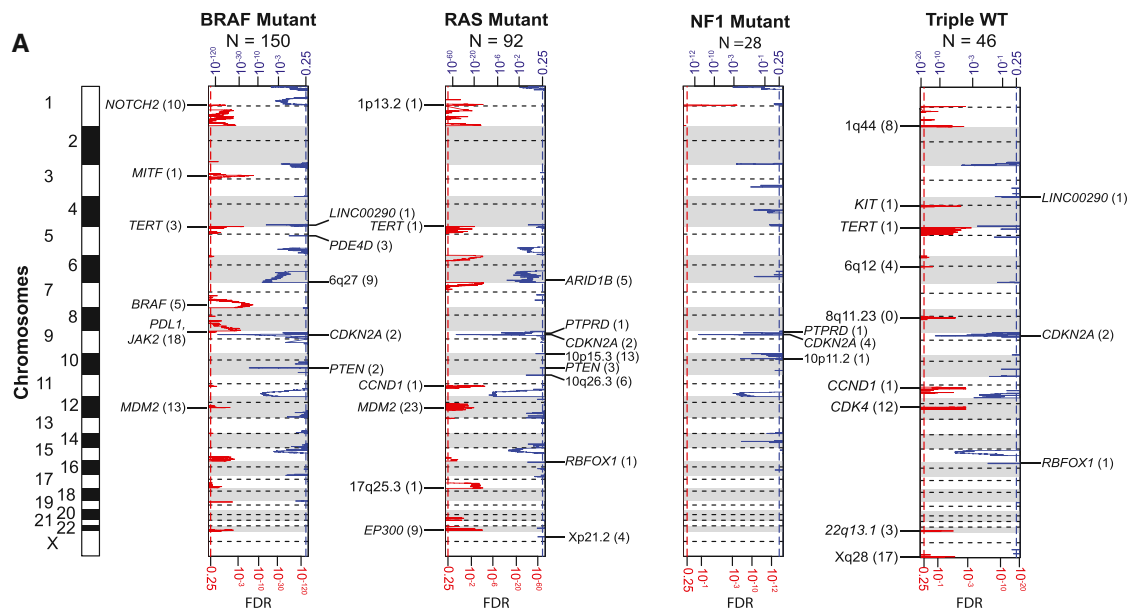
(legend on next page)

ShatterSeek followed by manual review (see Supplemental Experimental Procedures), we identified complex rearrangement events in 38% of samples (45/117) (Table S1D). Like fusion events, complex structural rearrangements were enriched in the Triple-WT subtype (11/16, Fisher's exact test p = 0.00098), particularly in those lacking a UV signature (7/7). Taken together with the pattern of somatic CNAs and the lower frequency of samples possessing a UV signature (~30%), these results suggest that, unlike other subtypes, other mutational processes that involve structural rearrangement of the genome drive the malignant phenotype of Triple-WT melanomas.

TERT Promoter Mutations

We confirmed mutually exclusive *TERT* promoter mutations C228T and C250T (Horn et al., 2013; Huang et al., 2013) in 23.5% and 40.9% of the 115 samples analyzed, respectively. Interestingly, only the C228T mutation was associated with elevated *TERT* mRNA expression (rank-sum test, p = 0.001) (Figure S2G) and contrasts with glioblastoma (GBM), in which both mutations were linked to increased expression (Brennan et al., 2013). *TERT* promoter mutations were observed in 75.0% (39/52) of *BRAF*, 71.9% (23/32) of *RAS*, and 83.3% (10/12) of *NF1* subtypes but in only 6.7% (1/15) of Triple-WT (p = 8e−5, Figure S2H), suggesting an alternative mechanism of TERT activation (e.g., *TERT* amplification or rearrangement; see above) in the Triple-WT melanomas.

CIMP Phenotype

While a higher frequency of *NRAS* hot-spot mutations (OR = 2.3, p = 0.003) and a lower frequency of *BRAF* hot-spot mutations (OR = 0.4, p = 0.0008) were found in the CIMP cluster defined by DNA methylation profiles (EEP), the strongest associations of CIMP were with *IDH1* (OR = 4.05, p = 0.005) and *ARID2* (OR = 3.5, p = 0.0003) mutations (Figure S1F), both of which are chromatin-remodeling genes. Those observations suggest that, despite the intriguing correlations, the CIMP phenotype is not driven by the events responsible for genotypic subtypes of melanoma.

Signaling Pathways

Classical signaling pathway diagrams suggest that *BRAF*, *RAS (N/H/K)*, and *NF1* subtypes share common downstream signaling. We analyzed RPPA profiles of 181 cancer-related total proteins and phosphoproteins in 200 melanoma samples to further assess downstream signaling among subtypes. Not surprisingly, components of the MAPK, PI(3)K, and apoptotic signaling pathways were differentially activated by *BRAF/RAS(N/H/K)/NF1* driver mutations (Figures 3 and S3). Although, for example, the upstream phospho-MAP2K1/MAP2K2 (MEK1/2) S217/S221 was elevated in both *BRAF* and *RAS* (N/H/K) hot-spot mutation subtypes (Figure 3A), the highest relative median activation of phospho-T202/Y204 MAPK1/MAPK3 (ERK1/2)

was observed in the *RAS* (N/H/K) mutant subgroup (Figure 3B). As predicted by copy-number analysis, Triple-WT tumors showed the highest median KIT protein abundance (Figure 3C). In contrast, *NF1* mutant melanomas had the highest median level of CRAF expression, highlighting differential MAPK activation in this subtype (Figure 3D). Other examples of differential subtype-specific signaling included higher median levels of the anti-apoptotic protein BCL-2 in the Triple-WT subtype (Figure 3E) and regulators of insulin signaling (IGFBP2) in *BRAF* hot-spot mutants (Figure 3F). Additional proteins involved in the PI(3)K/mTOR and epithelial-mesenchymal transition pathways were also significantly associated with particular mutation subtypes (Figure S3).

Molecular Pathways

To broaden our view of the common molecular processes dysregulated in melanoma, we integrated mutation, copy-number, and methylation data to identify recurrently targeted pathways and signaling interactions involving significantly altered genes in all samples (n = 318) (Figures S4A–S4D). We manually curated the genetic alterations by *BRAF*, *RAS* (N/H/K), *NF1*, and Triple-WT subtypes (Figure 4A) and found that RAS (N/H/K)-MAPK-AKT, RB1/CDKN2A cell-cycle pathways, and MDM2/TP53 apoptosis pathways were altered in 91%, 69%, and 19% of cases, respectively. *TP53* mutations were found more frequently in *BRAF*, *RAS*, and *NF1* tumors, compared to Triple-WT, in which *MDM2* amplifications were more frequent. Interestingly, of the 49 *TP53* mutations identified, 46 (93.9%) were found in UV signature samples. Although *CDKN2A/B* alterations were nearly evenly distributed across subtypes, *CDK4* and *CCND1* amplifications were more frequent in Triple-WTs, and *RB1* mutations were detected in a higher fraction of *NF1* subtype tumors. Of the 12 *RB1* mutations identified in this study, all were in UV signature samples. Finally, as previously reported (Pollock et al., 2003), *PTEN* mutations and deletions were more frequent in *BRAF*-mutant melanomas (Figures 4A and 4B), whereas amplification and mRNA overexpression of AKT3 were significantly enriched in *RAS* (N/H/K), *NF1*, and Triple-WT compared to the *BRAF* subtype (p < 0.05) (Figure 4B).

Transcriptomic Classification of Melanoma

We performed consensus hierarchical clustering analysis (TCGA, 2014a) of the 1,500 genes with the most variant expression levels in 329 samples and identified three robust stable clusters. Based on the gene function(s) of discriminatory mRNA transcripts, we named the clusters "immune" (n = 168; 51%), "keratin" (n = 102; 31%), and "MITF-low" (n = 59; 18%) (Figure 5A and Table S4A). Interestingly, post-accession survival of patients with regionally metastatic tumors was significantly different among the three clusters

---

Figure 2. Landscape of Copy-Number Alterations in Melanoma
(A) GISTIC 2 analysis across four subtypes with selected highlighted genes from significant minimal common regions.
(B) Fraction of *BRAF*, *RAS (N/H/K)*, *NF1*, and Triple-WT subtypes with focal amplifications determined by GISTIC 2 for *BRAF* and *MITF* (left) and *KIT*, *PDGFRA*, *KDR*, *MDM2*, *CDK4*, *CCND1*, and *TERT* (right). Asterisk indicates significant increase in amplification in the indicated mutation subtype compared to the rest by Fisher's exact test (p < 0.01, FDR < 0.05).
(C) Landscape of mutation subtypes, selected cosmic mutations, and subtype-specific enriched copy-number amplifications. Per sample mutation rate, age, and mutation subtype (*BRAF*, *RAS*, *NF1*, and Triple-WT) (top), color-coded matrix of individual mutations and amplifications (specific *BRAF* and *NRAS* mutations indicated) (middle), and type of melanoma specimen (primary or metastasis) and mutation spectra for all samples (bottom) are shown.
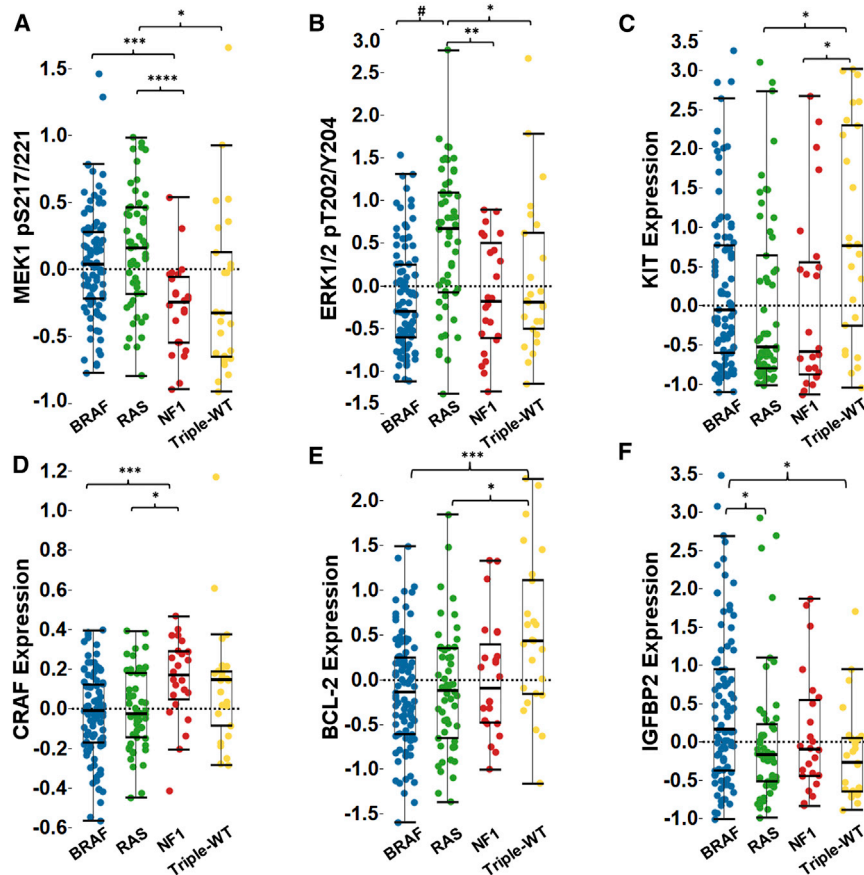See also Figure S2.

Figure 3. Analysis of Protein Expression Levels in Melanoma Samples

Individual protein levels were determined by RPPA across mutation subtypes.

(A) Phospho-MAP2K1/MAP2K2 (MEK1/2) S217/S221 was elevated in both the *BRAF* and *RAS* hot-spot mutation subtypes compared to NF1 and Triple-WT.

(B) Only *RAS* hot-spot mutant samples showed higher median levels of phospho-T202 Y204 MAPK1/MAPK3 (ERK1/2).

(C) Triple-WT melanomas had the highest median KIT protein expression.

(D and E) (D) *NF1* mutant melanomas had a higher median level of CRAF expression, and Triple-WT had higher BCL-2 levels (E) compared to *BRAF* and *RAS* subtypes.

(F) Median IGFBP2 levels were highest in *BRAF* hot-spot mutant samples. Kruskal-Wallis test, and the post hoc Kruskal Nemenyi test for pairwise comparisons.

$*p < 0.05$, $**p < 0.01$, $***p < 0.005$, $****p < 0.001$, $\#p = 5.4e-6$. See also Figure S3.

(p = 0.001, Figure 5B), suggesting that these transcriptomically defined subclasses may be biologically relevant and distinct.

"Immune" Subclass

A significant number of genes overexpressed in this subclass were associated with immune cell subsets (T cells, B cells, and NK cells), immune signaling molecules, co-stimulatory and co-inhibitory immune checkpoint proteins, cytokines, chemokines, and corresponding receptors (Tables S4A–S4B). As 74% (113/152) of samples in the subclass were procured from regional lymph nodes (Pearson's chi-square test, p < 0.001), we first assessed whether high expression of immune-related genes reflected the biology of melanoma-infiltrating immune cells or a non-specific admixture of "contaminating" adjacent lymphoid tissue in the samples (Erdag et al., 2012). Specifically, we compared the expression of nine curated immune gene signatures (comprising 793 genes and detailed in Table S4B) in 172 samples from lymph nodes and 157 tumors from other tissues (Figures S5A and S5B). Reassuringly, there was no significant difference in expression of tested immune signatures between the samples from lymph nodes and non-lymph node tissues (Figure S5A), suggesting that the transcriptomic features of the immune subclass were not due to contaminating adjacent lymph node tissue. Patients with regionally metastatic tumors in this subclass showed more favorable post-accession survival than did those

in the other two subclasses (log-rank test, p = 0.003), in accordance with previous reports of the host immune response in melanoma (Azimi et al., 2012).

"Keratin" Subclass

This cluster was characterized by high expression of genes associated with keratins, pigmentation, and epithelium, as well as genes associated with neuronal development or other organ-specific embryologic development (Table S4A). Approximately 74% of primary melanomas clustered within this group (Pearson's chi-square test, p < 0.001) and showed high expression of genes previously reported to be elevated in primary melanomas. Included were several keratins, kallikreins, and other epidermal genes. However, 25 keratin cluster samples were derived from regional lymph nodes, suggesting that expression of the epithelial transcripts was not due solely to admixture of epithelial tissue (such as skin epidermis) with melanoma tumor tissue, at least for this organ site of procurement; indeed, keratins and other epithelial markers have been found in some melanoma cell lines (Shields et al., 2007). Of note, regional metastatic melanomas exhibited worse outcome when compared with stage-matched samples assigned to the immune or MITF-low cluster (log-rank, p = 0.0007) (Figure 5B), supporting the view that the keratin cluster represents, at least in part, a previously unappreciated but biologically distinct melanoma subtype with adverse prognosis.

"MITF-Low" Subclass

The "MITF-low" cluster was characterized by low expression of genes associated with pigmentation and epithelial expression (Table S4A), including several MITF target genes and genes involved in immunomodulation, adhesion, migration, and extracellular matrix. This cluster was significantly enriched with genes preferentially expressed within the nervous system and/or
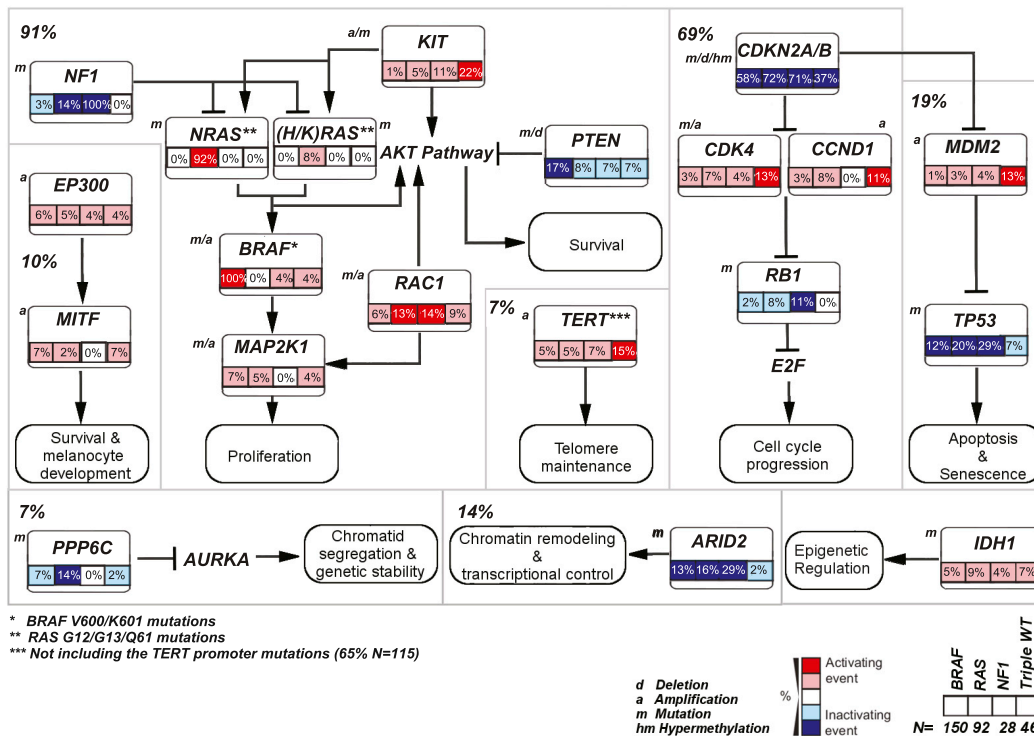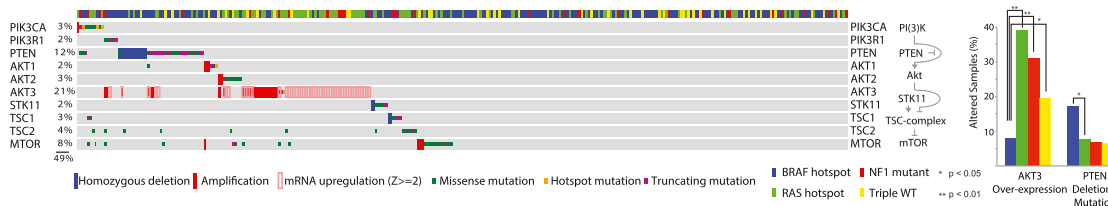
Figure 4. Pathways Altered in Melanoma

(A) Percentage of recurrently altered pathways in the four melanoma subtypes (*BRAF* = V600/K601 mutants, *RAS* [*N/H/K*] = G12, G13, and Q61 mutants) through integration of mutation, copy-number variation, and hypermethylation data are indicated (n = 316; not shown are one hyper-mutated and one co-occurring *BRAF/NRAS* hot-spot mutant sample). Manual curated pathway shows percentage of TP53, CDKN2A/RB1, and MAPK/AKT pathway across all samples (note: percentages of alterations of MAPK and AKT pathway are combined, given their high level of interconnectivity). a, amplification; d, deletion, m, mutation.

(B) Co-occurring somatic CNAs, mutations, and mRNA expression (color code indicated on graph) for the PI(3)K/mTOR pathway across the four mutation subtypes (left). Bar graph indicating percentage of fraction of subtypes with *AKT3* activation or *PTEN* inactivation (right). Enrichment of a given alteration in a subgroup is estimated by Fisher's exact test.

See also Figure S4.

associated with neuronal development or other organ-specific embryologic development.

Integrative Molecular Subtypes

Using the iCluster algorithm (see Supplemental Experimental Procedures), we next integrated multiple genomic dimensions (mutation, somatic CNAs, DNA methylation, and expression) to define molecular subtypes and to unravel hidden associations of the various subtypes identified in each genomic dimension (Figures 5A, S1D, S5C, and S7 and Data S1 and Table S4). We observed clear associations between the keratin expression subtype, the CIMP subtype, and a miRNA subgroup (cluster 3),

which had a relatively lower frequency of hot-spot *BRAF* mutations (Figure S5D, iClust 1). Conversely, "MITF-low" cluster samples had a higher percentage of *BRAF*-hot-spot mutations (compared with "keratin" and "immune" clusters: 66% versus 33% and 45%, respectively; Fisher's exact test, p = 0.0003 (visualized in Figure S5E). In addition, a lower percentage of tumor samples that were classified as "MITF-low" had no mutations in either *BRAF*, *NRAS*, and *NF1* compared with "keratin" and "immune" clusters (3% versus 21% and 14%, respectively; Fisher's exact test, p = 0.006) (Figure S5E). We also discerned associations with the hypomethylation subgroup and the MITF
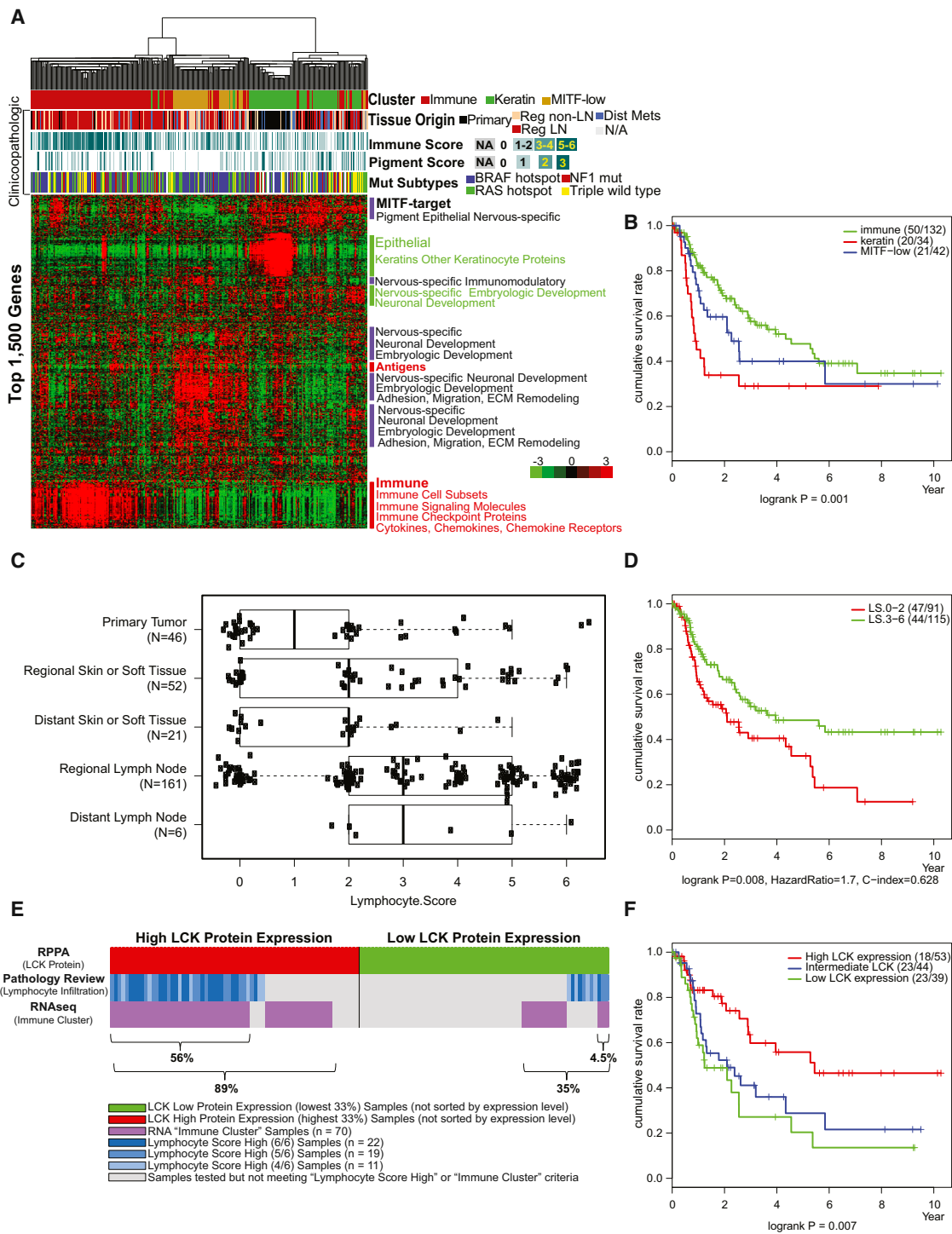
Figure 5. Integrative Analysis across Multiple Molecular Data Platforms Provides Insights into the Biology and Prognostic Significance of Immune Infiltrates in Cutaneous Melanoma

(A and B) (A) Unsupervised clustering of 329 melanoma samples using the top 1,500 genes showing the maximum absolute deviation identify three clusters defined as "immune-high," "keratin-high," and "microphthalmia-associated transcription factor (MITF)-low" based on gene function of discriminatory mRNAs and (B) post-accession survival curves for RNA subgroups.

(C) Distribution of lymphocytic scores determined by histopathology analysis according to sample type (described in detail in the Supplemental Experimental Procedures).

(D) Post-accession survival curves for high and low lymphocytic infiltration scores.

(legend continued on next page)

expression class (Figure S5D, iClust 2). Finally, we observed a low copy-number subgroup, a normal-like methylation profile, and enrichment for tumors possessing the immune mRNA expression signature, consistent with the presence of lymphocytic infiltration (Figure S5D, iClust 3).

Clinical Significance of the Immune Transcriptomic Subclass

Demonstrating the clinical relevance of molecular classification requires interpretation in the context of existing clinical practice. As a proof of concept, we addressed the clinical relevance and potential application of the observation that the "immune" transcriptomic subclass was associated with improved post-accession survival of patients with regional metastatic melanoma.

Although tumor-infiltrating lymphocytes have been associated with favorable prognosis in primary melanoma (Azimi et al., 2012), such an association has not been investigated in regional disease. To assess whether our transcriptomic classification of melanoma captures the biology of tumor-associated lymphocytes, we complemented the clinicopathological annotation provided by tissue source sites with a standardized pathology review of frozen section slides by TCGA Analysis Working Group (AWG) dermatopathologists (see Author Contributions); the density and distribution of melanoma-associated lymphocytes were used to derive a "lymphocyte score" (LScore), a semiquantitative measure of the number of lymphocytes in a sample (see Supplemental Experimental Procedures). Additional histopathological parameters included percent tumor content, percent necrotic tissue, and amount of melanin pigment. Melanomas from regional or distant lymph nodes showed significantly higher LScore than tumors from other tissues (Wilcoxon rank-sum test, p = 5.6e−8; Figure 5C). Among the subgroup of regional metastatic melanomas, elevated LScore was significantly associated with prolonged post-accession survival (Figure 5D), corroborating prior observations that tumor-associated lymphocytes are a favorable prognostic factor in melanoma (Bogunovic et al., 2009; Mihm et al., 1996). Remarkably, there was a striking concordance between high LScore (3–6) and assignment to the immune subclass (Figure S6A) (Fisher's exact test, p < 1e−12).

Next, we asked whether transcriptomic features that defined the "immune" cluster are seen at the protein level by RPPA. In particular, we focused on two immune-related proteins, LCK and SYK, non-receptor tyrosine kinases commonly associated with T- and B-lymphocyte signaling. Interestingly, unsupervised clustering of RPPA data revealed that LCK and SYK are highly expressed in a subset of samples (Figure S5C) that are enriched with tumors in the transcriptomic immune subclass and/or that have high LScores (Figure 5E). However, high LCK, but not SYK, protein expression was also strongly associated with favorable post-accession survival of patients with regionally metastatic tumors (Figure 5F and data not shown). Tumors with high LScores tended to be assigned to the transcriptomic immune

subclass and also express elevated levels of LCK protein (Figures S6A and S6B). These three characteristics overlapped considerably, and a combination of the three predicted melanoma outcome more accurately than did any one of the features alone (log-rank, p = 8.0e−6, post-accession survival in regionally metastatic tumors; Figure S6C). This observation is consistent with the hypothesis that the three reflect unique (although overlapping) biological characteristics, each of which confers favorable outcomes in melanoma.

Finally, recognizing that unsupervised cluster analysis of a transcriptomic profile is not readily applicable to clinical practice, we tested the hypothesis that a bivariate model of LScore and LCK protein expression level offers a comparable prognostic prediction. Indeed, tumors with high LScore and high LCK expression were associated with significantly improved post-accession survival compared with those having low LScore and low LCK expression (log-rank p = 7.9e−5, hazard ratio = 5.5, tumors with both high LScore and LCK versus both scores low; Figure S6D). Multivariable Cox proportional hazard regression also demonstrated that both LScore and LCK expression have independent predictive value in the two-factor model (Figure S6E). Overall, this integrative analysis suggests that a combination of LCK protein expression and pathologists' scoring of tumor-infiltrating lymphocytes may be more prognostic for patients with nodal metastases than assessment of tumor-infiltrating lymphocytes alone.

DISCUSSION

We propose here that cutaneous melanomas can be divided into four genomic subtypes, designated *BRAF*, *RAS (N/H/K)*, *NF1*, and Triple-WT. Such a genomic classification provides a framework for exploring how additional molecular alterations may explain observed biological and clinical differences among the subtypes. It also provides signposts for identification of drugable targets and predictive biomarkers, as well as potentially useful guidance for decisions about therapy.

Based on evidence that (1) *BRAF/RAS (N/H/K)* mutant melanomas are driven, at least in part, by MAPK signaling (Hodis et al., 2012; Krauthammer et al., 2012); (2) melanomas lacking NF1 expression are dependent on MAPK signaling and respond to MAPK inhibitors (Maertens et al., 2013; Nissan et al., 2014); and (3) there are clinicopathologic and molecular differences among melanomas that do not have hot-spot mutations in *BRAF/RAS* but differ with respect to *NF1* mutation status, melanoma joins two other RTK/RAS-driven solid tumor types (GBM and lung adenocarcinoma) analyzed by the TCGA, among which a subset of these cancers has loss-of-function *NF1* mutations (TCGA, 2008, 2014b).

We suggest that significantly mutated genes and other molecular alterations identified here, combined with previously described melanoma-associated genes, are likely to have

---

(E) Overlap of LCK high and low protein expression obtained from RPPA data with lymphocytic infiltration scores determined by pathology and RNA immune subgroups determined by mRNA clustering analysis.

(F) Association of LCK protein with post-accession survival. Three curves describe cumulative survival rates of three tertile patient subsets (p = 0.007 with log-rank test).

See also Figures S5, S6, and S7 and Data S1.

important implications for prognosis and therapy (Table 1). For example, we postulate that patients with *BRAF* wild-type, *NF1* mutant melanomas respond to MEK and/or ERK inhibitors (Maertens et al., 2013; Nissan et al., 2014; Whittaker et al., 2013), supported by cell line studies that demonstrate that at least some *NF1* mutant cell lines respond to MEK inhibitors (Ranzani et al., 2015). In the setting of frequently co-occurring *NF1* and *ARID2* mutations, synthetic lethal strategies targeting chromatin modifiers represent a rational area for pre-clinical research (Helming et al., 2014). In addition to therapeutic strategies currently under clinical development, melanomas with *RAS (N/H/K)* mutations, frequently concurrent with *PPP6C* hot-spot mutations, may provide therapeutic opportunities for combinatorial treatment strategies that include Aurora kinase inhibition (Gold et al., 2014). Previous studies have shown frequent co-occurrence of *BRAF* mutations and *PTEN* mutations or deletions (Tsao et al., 2012). Here, we showed a higher frequency of amplifications and overexpression of AKT3 in *RAS*, *NF1*, and Triple-WT melanomas, which may provide additional biomarkers to support the use of combination MEK and PI(3)K/AKT/mTOR pathway inhibitors in such subtypes. In addition, mutations in *PIK3CA* (E545K, H1047L) and *AKT1/3* (E17K) in *BRAF*, as well as *RAS (N/H/K)* mutant melanoma (Table S2E), may serve as biomarkers that predict response to the above-mentioned targeted therapies.

Candidate driver events in Triple-WT melanomas provide opportunities for pre-clinical and clinical efforts to effectively target these molecular aberrations. These include *KIT* mutations/amplifications, co-amplified RTKs, *PDGFRA* and *KDR* (*VEGFR2*), and even rare *GNAQ* Q209P (n = 1) and *GNA11* Q209L (n = 2) mutations (sample IDs: TCGA-ER-A3ES, TCGA-ER-A3ET, and TCGA-ER-A2NF)—the latter of which, interestingly, co-occur with hot-spot *SF3B1* R625H mutations (n = 2 for co-occurrence with GNA11/Q hot-spot mutations) in our cutaneous melanoma cohort, but not *BAP1* mutations, which are frequently found in metastatic uveal melanoma (Field and Harbour, 2014). Although *GNAQ* and *GNA11* hot-spot mutations are common in uveal melanomas, they have also been reported in blue nevi and primary melanocytic neoplasms of the central nervous system (Küsters-Vandevelde et al., 2010). Our classification supports the use of imatinib and dasatinib to treat patients with *KIT*-mutated/amplified cutaneous melanomas (Carvajal et al., 2011; Hodi et al., 2008; Lutzky et al., 2008; Terheyden et al., 2010) and consideration of combination therapies with sorafenib, crenolanib, regorafenib, and pazopanib to target co-amplified RTKs, *PDGFRA*, and *KDR* (*VEGFR2*). Triple-WT melanomas with amplifications of *MDM2* and overexpression of BCL2 may respond to inhibitors such as AMG 232, nutlin-3, and BH3 mimetics, currently in preclinical or clinical development in melanoma. Such agents may also be beneficial for patients with wild-type *TP53* across the genetic subtypes (Frederick et al., 2014; Ji et al., 2013; Sun et al., 2014). Other potentially actionable mutations include recurrent *IDH1* R132 (~6%) and *EZH2* Y641 mutations (<1%) (Table S2E).

Overall, approximately half of all cases were assigned to the "immune" subtype. Interestingly, the response rate to inhibitors of the PD-1/PD-L1 pathway is approximately one-third (Brahmer et al., 2012; Hamid et al., 2013; Topalian et al., 2012). In our

study, expression of both PD-1 and PD-L1 was significantly higher in "immune" compared to each of the two other groups (Figure S6F), similar to a recent report showing that pre-existing CD8+ T cells distinctly located at the invasive tumor margin are associated with immunohistochemical expression of PD-1 and PD-L1, and was also predictive of response to pembrolizumab (Tumeh et al., 2014). However, it is important to emphasize that our data do not prove that the immune subtype represents a population responsive to immunotherapies.

We show that immune infiltration is statistically correlated with more favorable prognosis, irrespective of genomic subtype. The lack of a genomic correlation with outcome provides a plausible molecular explanation for the lack of observed preferential antitumor responses in clinical trials employing immune checkpoint blockade, at least in relation to *BRAF* status (Ascierto et al., 2014; Robert et al., 2014). Nonetheless, despite these data, the question of whether specific mutated melanoma antigens are responsible for differences in the degree of tumor infiltration by lymphocytes is an area of active investigation (Robbins et al., 2013; Snyder et al., 2014). Our combined RPPA analysis, including exploration of LCK and SYK proteins that are associated with T cell and B cell signaling effectors, respectively, suggests that T cell, but not B cell, signaling has prognostic significance. This relevance of T cells, and in particular effector CD8+ T cells, is congruent with clinical benefit seen with high-dose bolus IL-2, a T cell growth factor used as a therapeutic agent for advanced melanoma (McArthur and Ribas, 2013).

Among the cohort of patients in this study with advanced stage III disease (Balch et al., 2010), high lymphocytic score and immune-associated gene expression was associated with prolonged post-accession survival, potentially reflecting a clinical benefit of immunotherapies for stage III melanoma patients (Eggermont et al., 2008; Kirkwood et al., 1996). Such markers should be considered for further evaluation and potential integration into future AJCC staging systems and associated prognostic models, as well as for exploration as a potential predictor of response to adjuvant therapies for stage III disease.

EXPERIMENTAL PROCEDURES

Patients and Biospecimens

Eligible patients had a diagnosis of either primary or metastatic cutaneous melanoma or metastatic melanoma of unknown primary (Balch et al., 2009; Dasgupta et al., 1963), but no previous systemic therapy (except that adjuvant interferon-α $\geq$90 days prior was permitted); the site from which the biospecimen was collected could not have been previously treated at any time with radiotherapy. Biospecimens from resected primary and/or metastatic melanomas were obtained from patients with appropriate informed consent and institutional review board or ethics board approval. Biospecimens were classified as either primary or metastatic based on the available clinical and pathological information. Independent pathological review confirmed that each biospecimen was consistent with melanoma. As specimens were required to have sufficient mass and quality for downstream molecular analyses, those from advanced primary and/or metastatic tumors were over-represented. The complete methodology for patient eligibility, clinical and pathological data elements, biospecimen acquisition, and molecular analyte extraction is described in the Supplemental Experimental Procedures.

Data Generation

Data from at least one platform were available for 333 patients. The data types included: (1) clinical, (2) whole-exome sequencing, (3) DNA copy-number and

single-nucleotide polymorphism array, (4) whole-genome sequencing, (5) RNA-sequencing data, (6) DNA methylation, (7) reverse-phase protein array, and (8) microRNA sequencing. Details of data generation and analyses are described in the Supplemental Experimental Procedures. All data sets are available through the Cancer Genome Atlas (TCGA) data portal (https://tcga-data.nci.nih.gov/tcga).

Whole-Genome and Exome-Sequencing Data Analysis

Whole-exome sequencing was performed as previously described (TCGA, 2012). Exome capture was performed using the Agilent Sure-Select Human All Exon v2.0, 44 Mb kit, followed by 2 × 76 bp paired-end sequencing on the Illumina HiSeq platform. Read alignment and processing were performed using BWA and the Picard and Firehose pipelines at the Broad Institute. For each file, Picard generates a single BAM file that includes reads, calibrated quantities, and alignments to the genome. The Firehose pipeline performs quality control, local realignment, mutation calling, small insertion and deletion identification, and coverage calculations, among other analyses. Complete details of the pipeline can be found online at http://www.broadinstitute.org/cancer/cga. Whole-genome sequencing methods are described in detail in the Supplemental Experimental Procedures.

RNA-Sequencing Data Analysis

Total RNA was converted to mRNA libraries using the Illumina mRNA TruSeq kit, following the manufacturer's directions. Libraries were sequenced on the Illumina HiSeq 2000 as previously described (TCGA, 2012). Read mapping, gene expression quantitation, and identification of fusion transcripts are described in the Supplemental Experimental Procedures.

SUPPLEMENTAL INFORMATION

Supplemental Information includes Supplemental Experimental Procedures, seven figures, four tables, and one data file and can be found with this article online at http://dx.doi.org/10.1016/j.cell.2015.05.044.

CONSORTIA

The members of The Cancer Genome Atlas Research Network for this project are Rehan Akbani, Kadir C. Akdemir, B. Arman Aksoy, Monique Albert, Adrian Ally, Samirkumar B. Amin, Harindra Arachchi, Arshi Arora, J. Todd Auman, Brenda Ayala, Julien Baboud, Miruna Balasundaram, Saianand Balu, Nandita Barnabas, John Bartlett, Boris C. Bastian, Stephen B. Baylin, Madhusmita Behera, Dmitry Belyaev, Christopher Benz, Brady Bernard, Rameen Beroukhim, Natalie Bir, Aaron D. Black, Tom Bodenheimer, Lori Boice, Genevieve M. Boland, Riccardo Bono, Moiz S. Bootwalla, Marcus Bosenberg, Jay Bowen, Reanne Bowlby, Christopher A. Bristow, Laura Brockway-Lunardi, Denise Brooks, Jakub Brzezinski, Wiam Bshara, Elizabeth Buda, William R. Burns, Yaron S.N. Butterfield, Michael Button, Tiffany Calderone, Giancarlo Antonini Cappellini, Candace Carter, Scott L. Carter, Lynn Cherney, Andrew D. Cherniack, Aaron Chevalier, Lynda Chin, Juok Cho, Raymond J. Cho, Yoon-La Choi, Andy Chu, Sudha Chudamani, Kristian Cibulskis, Giovanni Ciriello, Amanda Clarke, Stephen Coons, Leslie Cope, Daniel Crain, Erin Curley, Ludmila Danilova, Stefania D'Atri, Tanja Davidsen, Michael A. Davies, Keith A. Delman, John A. Demchok, Qixia A. Deng, Yonathan Lissanu Deribe, Noreen Dhalla, Rajiv Dhir, Daniel DiCara, Michael Dinikin, Michael Dubina, J. Stephen Ebrom, Sophie Egea, Greg Eley, Jay Engel, Jennifer M. Eschbacher, Konstantin V. Fedosenko, Ina Felau, Timothy Fennell, Martin L. Ferguson, Sheila Fisher, Keith T. Flaherty, Scott Frazer, Jessica Frick, Victoria Fulidou, Stacey B. Gabriel, Jianjiong Gao, Johanna Gardner, Levi A. Garraway, Julie M. Gastier-Foster, Carmelo Gaudioso, Nils Gehlenborg, Giannicola Genovese, Mark Gerken, Jeffrey E. Gershenwald, Gad Getz, Carmen Gomez-Fernandez, Thomas Gribbin, Jonna Grimsby, Benjamin Gross, Ranabir Guin, Tony Gutschner, Angela Hadjipanayis, Ruth Halaban, Benjamin Hanf, David Haussler, Lauren E. Haydu, D. Neil Hayes, Nicholas K. Hayward, David I. Heiman, Lynn Herbert, James G. Herman, Peter Hersey, Katherine A. Hoadley, Eran Hodis, Robert A. Holt, Dave SB Hoon, Susan Hoppough, Alan P. Hoyle, Franklin W. Huang, Mei Huang, Sharon Huang, Carolyn M. Hutter, Matthew Ibbs, Lisa Iype, Anders Jacobsen, Valerie Jakrot, Alyssa Janning, William R. Jeck, Stuart R. Jefferys, Mark A. Jensen, Corbin D. Jones, Steven J.M. Jones, Zhenlin Ju, Hojabr Kakavand, Hyojin Kang, Richard F. Kefford, Fadlo R. Khuri, Jaegil Kim, John M. Kirkwood, Joachim Klode, Anil Korkut, Konstanty Korski, Michael Krauthammer, Raju Kucherlapati, Lawrence N. Kwong, Witold Kycler, Marc Ladanyi, Phillip H. Lai, Peter W. Laird, Eric Lander, Michael S. Lawrence, Alexander J. Lazar, Radoslaw Łaźniak, Darlene Lee, Jeffrey E. Lee, Junehawk Lee, Kenneth Lee, Semin Lee, William Lee, Ewa Leporowska, Kristen M. Leraas, Haiyan I. Li, Tara M. Lichtenberg, Lee Lichtenstein, Pei Lin, Shiyun Ling, Jia Liu, Ouida Liu, Wenbin Liu, Georgina V. Long, Yiling Lu, Singer Ma, Yussanne Ma, Andrzej Mackiewicz, Harshad S. Mahadeshwar, Jared Malke, David Mallery, Georgy M. Manikhas, Graham J. Mann, Marco A. Marra, Brenna Matejka, Michael Mayo, Sousan Mehrabi, Shaowu Meng, Matthew Meyerson, Piotr A. Mieczkowski, John P. Miller, Martin L. Miller, Gordon B. Mills, Fedor Moiseenko, Richard A. Moore, Scott Morris, Carl Morrison, Donald L. Morton, Stergios Moschos, Lisle E. Mose, Florian L. Muller, Andrew J. Mungall, Dawid Murawa, Pawel Murawa, Bradley A. Murray, Luigi Nezi, Sam Ng, Dana Nicholson, Michael S. Noble, Adeboye Osunkoya, Taofeek K. Owonikoko, Bradley A. Ozenberger, Elena Pagani, Oxana V. Paklina, Angeliki Pantazi, Michael Parfenov, Jeremy Parfitt, Peter J. Park, Woong-Yang Park, Joel S. Parker, Francesca Passarelli, Robert Penny, Charles M. Perou, Todd D. Pihl, Olga Potapova, Victor G. Prieto, Alexei Protopopov, Michael J. Quinn, Amie Radenbaugh, Kunal Rai, Suresh S. Ramalingam, Ayush T. Raman, Nilsa C. Ramirez, Ricardo Ramirez, Uma Rao, W. Kimryn Rathmell, Xiaojia Ren, Sheila M. Reynolds, Jeffrey Roach, A. Gordon Robertson, Merrick I. Ross, Jason Roszik, Giandomenico Russo, Gordon Saksena, Charles Saller, Yardena Samuels, Chris Sander, Cindy Sander, George Sandusky, Netty Santoso, Melissa Saul, Robyn PM Saw, Dirk Schadendorf, Jacqueline E. Schein, Nikolaus Schultz, Steven E. Schumacher, Charles Schwallier, Richard A. Scolyer, Jonathan Seidman, Pedamallu Chandra Sekhar, Harmanjatinder S. Sekhon, Yasin Senbabaoglu, Sahil Seth, Kerwin F. Shannon, Samantha Sharpe, Norman E. Sharpless, Kenna R. Mills Shaw, Candace Shelton, Troy Shelton, Ronglai Shen, Margi Sheth, Yan Shi, Carolyn J Shiau, Ilya Shmulevich, Gabriel L. Sica, Janae V. Simons, Rileen Sinha, Payal Sipahimalani, Heidi J. Sofia, Matthew G. Soloway, Xingzhi Song, Carrie Sougnez, Andrew J. Spillane, Arkadiusz Spychała, Jonathan R. Stretch, Joshua Stuart, Wiktoria M. Suchorska, Antje Sucker, S. Onur Sumer, Yichao Sun, Maria Synott, Barbara Tabak, Teresa R. Tabler, Angela Tam, Donghui Tan, Jiabin Tang, Roy Tarnuzzer, Katherine Tarvin, Honorata Tatka, Barry S. Taylor, Marek Teresiak, Nina Thiessen, John F. Thompson, Leigh Thorne, Vesteinn Thorsson, Jeffrey M. Trent, Timothy J. Triche, Jr., Kenneth Y. Tsai, Peiling Tsou, David J. Van Den Berg, Eliezer M. Van Allen, Umadevi Veluvolu, Roeland G. Verhaak, Douglas Voet, Olga Voronina, Vonn Walter, Jessica S. Walton, Yunhu Wan, Yuling Wang, Zhining Wang, Scot Waring, Ian R. Watson, Nils Weinhold, John N. Weinstein, Daniel J. Weisenberger, Peter White, Matthew D. Wilkerson, James S. Wilmott, Lisa Wise, Maciej Wiznerowicz, Scott E. Woodman, Chang-Jiun Wu, Chia-Chin Wu, Junyuan Wu, Ye Wu, Ruibin Xi, Andrew Wei Xu, Da Yang, Liming Yang, Lixing Yang, Travis I. Zack, Jean C. Zenklusen, Hailei Zhang, Jianhua Zhang, Wei Zhang, Xiaobei Zhao, Jingchun Zhu, Kelsey Zhu, Lisa Zimmer, Erik Zmuda, and Lihua Zou.

AUTHOR CONTRIBUTIONS

The Cancer Genome Atlas Research Network contributed collectively to this study. Biospecimens were provided by the tissue source sites and processed by the Biospecimen Core Resource. Data generation and analyses were performed by the genome-sequencing centers, cancer genome-characterization centers, and genome data analysis centers. All data were released through the Data Coordinating Center. The NCI and NHGRI project teams coordinated project activities. Individual contributions of TCGA investigators are detailed in the Supplemental Information.

ACKNOWLEDGMENTS

REFERENCES

Andersen, L.B., Fountain, J.W., Gutmann, D.H., Tarlé, S.A., Glover, T.W., Dracopoli, N.C., Housman, D.E., and Collins, F.S. (1993). Mutations in the neurofibromatosis 1 gene in sporadic malignant melanoma cell lines. Nat. Genet. *3*, 118–121.

Ascierto, P.A., Simeone, E., Sileni, V.C., Pigozzo, J., Maio, M., Altomonte, M., Del Vecchio, M., Di Guardo, L., Marchetti, P., Ridolfi, R., et al. (2014). Clinical experience with ipilimumab 3 mg/kg: real-world efficacy and safety data from an expanded access programme cohort. J. Transl. Med. *12*, 116.

Azimi, F., Scolyer, R.A., Rumcheva, P., Moncrieff, M., Murali, R., McCarthy, S.W., Saw, R.P., and Thompson, J.F. (2012). Tumor-infiltrating lymphocyte grade is an independent predictor of sentinel lymph node status and survival in patients with cutaneous melanoma. J. Clin. Oncol. *30*, 2678–2683.

Baade, P., Meng, X., Youlden, D., Aitken, J., and Youl, P. (2012). Time trends and latitudinal differences in melanoma thickness distribution in Australia, 1990-2006. Int. J. Cancer *130*, 170–178.

Balch, C.M., Gershenwald, J.E., Soong, S.J., Thompson, J.F., Atkins, M.B., Byrd, D.R., Buzaid, A.C., Cochran, A.J., Coit, D.G., Ding, S., et al. (2009). Final version of 2009 AJCC melanoma staging and classification. J. Clin. Oncol. *27*, 6199–6206.

Balch, C.M., Gershenwald, J.E., Soong, S.J., Thompson, J.F., Ding, S., Byrd, D.R., Cascinelli, N., Cochran, A.J., Coit, D.G., Eggermont, A.M., et al. (2010). Multivariate analysis of prognostic factors among 2,313 patients with stage III melanoma: comparison of nodal micrometastases versus macrometastases. J. Clin. Oncol. *28*, 2452–2459.

Berger, M.F., Hodis, E., Heffernan, T.P., Deribe, Y.L., Lawrence, M.S., Protopopov, A., Ivanova, E., Watson, I.R., Nickerson, E., Ghosh, P., et al. (2012). Melanoma genome sequencing reveals frequent PREX2 mutations. Nature *485*, 502–506.

Bogunovic, D., O'Neill, D.W., Belitskaya-Levy, I., Vacic, V., Yu, Y.L., Adams, S., Darvishian, F., Berman, R., Shapiro, R., Pavlick, A.C., et al. (2009). Immune profile and mitotic index of metastatic melanoma lesions enhance clinical staging in predicting patient survival. Proc. Natl. Acad. Sci. USA *106*, 20429–20434.

Brahmer, J.R., Tykodi, S.S., Chow, L.Q., Hwu, W.J., Topalian, S.L., Hwu, P., Drake, C.G., Camacho, L.H., Kauh, J., Odunsi, K., et al. (2012). Safety and activity of anti-PD-L1 antibody in patients with advanced cancer. N. Engl. J. Med. *366*, 2455–2465.

Brash, D.E. (2015). UV signature mutations. Photochem. Photobiol. *91*, 15–26.

Brennan, C.W., Verhaak, R.G., McKenna, A., Campos, B., Noushmehr, H., Salama, S.R., Zheng, S., Chakravarty, D., Sanborn, J.Z., Berman, S.H., et al.;

TCGA Research Network (2013). The somatic genomic landscape of glioblastoma. Cell *155*, 462–477.

Carter, S.L., Cibulskis, K., Helman, E., McKenna, A., Shen, H., Zack, T., Laird, P.W., Onofrio, R.C., Winckler, W., Weir, B.A., et al. (2012). Absolute quantification of somatic DNA alterations in human cancer. Nat. Biotechnol. *30*, 413–421.

Carvajal, R.D., Antonescu, C.R., Wolchok, J.D., Chapman, P.B., Roman, R.A., Teitcher, J., Panageas, K.S., Busam, K.J., Chmielowski, B., Lutzky, J., et al. (2011). KIT as a therapeutic target in metastatic melanoma. JAMA *305*, 2327–2334.

Criscione, V.D., and Weinstock, M.A. (2010). Melanoma thickness trends in the United States, 1988-2006. J. Invest. Dermatol. *130*, 793–797.

Curtin, J.A., Fridlyand, J., Kageshita, T., Patel, H.N., Busam, K.J., Kutzner, H., Cho, K.H., Aiba, S., Bröcker, E.B., LeBoit, P.E., et al. (2005). Distinct sets of genetic alterations in melanoma. N. Engl. J. Med. *353*, 2135–2147.

Dasgupta, T., Bowden, L., and Berg, J.W. (1963). Malignant Melanoma of Unknown Primary Origin. Surg. Gynecol. Obstet. *117*, 341–345.

Draper, G.J., Sanders, B.M., and Kingston, J.E. (1986). Second primary neoplasms in patients with retinoblastoma. Br. J. Cancer *53*, 661–671.

Dutton-Regester, K., Gartner, J.J., Emmanuel, R., Qutob, N., Davies, M.A., Gershenwald, J.E., Robinson, W., Robinson, S., Rosenberg, S.A., Scolyer, R.A., et al. (2014). A highly recurrent RPS27 5′UTR mutation in melanoma. Oncotarget *5*, 2912–2917.

Eggermont, A.M., Suciu, S., Santinami, M., Testori, A., Kruit, W.H., Marsden, J., Punt, C.J., Salès, F., Gore, M., Mackie, R., et al.; EORTC Melanoma Group (2008). Adjuvant therapy with pegylated interferon alfa-2b versus observation alone in resected stage III melanoma: final results of EORTC 18991, a randomised phase III trial. Lancet *372*, 117–126.

Erdag, G., Schaefer, J.T., Smolkin, M.E., Deacon, D.H., Shea, S.M., Dengel, L.T., Patterson, J.W., and Slingluff, C.L., Jr. (2012). Immunotype and immunohistologic characteristics of tumor-infiltrating immune cells are associated with clinical outcome in metastatic melanoma. Cancer Res. *72*, 1070–1080.

Field, M.G., and Harbour, J.W. (2014). Recent developments in prognostic and predictive testing in uveal melanoma. Curr. Opin. Ophthalmol. *25*, 234–239.

Frederick, D.T., Salas Fragomeni, R.A., Schalck, A., Ferreiro-Neira, I., Hoff, T., Cooper, Z.A., Haq, R., Panka, D.J., Kwong, L.N., Davies, M.A., et al. (2014). Clinical profiling of BCL-2 family members in the setting of BRAF inhibition offers a rationale for targeting de novo resistance using BH3 mimetics. PLoS ONE *9*, e101286.

Gershenwald, J.E., and Ross, M.I. (2011). Sentinel-lymph-node biopsy for cutaneous melanoma. N. Engl. J. Med. *364*, 1738–1745.

Gold, H.L., Wengrod, J., de Miera, E.V., Wang, D., Fleming, N., Sikkema, L., Kirchhoff, T., Hochman, T., Goldberg, J.D., Osman, I., and Gardner, L.B. (2014). PP6C hotspot mutations in melanoma display sensitivity to Aurora kinase inhibition. Mol. Cancer Res. *12*, 433–439.

Hamid, O., Robert, C., Daud, A., Hodi, F.S., Hwu, W.J., Kefford, R., Wolchok, J.D., Hersey, P., Joseph, R.W., Weber, J.S., et al. (2013). Safety and tumor responses with lambrolizumab (anti-PD-1) in melanoma. N. Engl. J. Med. *369*, 134–144.

Helming, K.C., Wang, X., Wilson, B.G., Vazquez, F., Haswell, J.R., Manchester, H.E., Kim, Y., Kryukov, G.V., Ghandi, M., Aguirre, A.J., et al. (2014). ARID1B is a specific vulnerability in ARID1A-mutant cancers. Nat. Med. *20*, 251–254.

Hodi, F.S., Friedlander, P., Corless, C.L., Heinrich, M.C., Mac Rae, S., Kruse, A., Jagannathan, J., Van den Abbeele, A.D., Velazquez, E.F., Demetri, G.D., and Fisher, D.E. (2008). Major response to imatinib mesylate in KIT-mutated melanoma. J. Clin. Oncol. *26*, 2046–2051.

Hodis, E., Watson, I.R., Kryukov, G.V., Arold, S.T., Imielinski, M., Theurillat, J.P., Nickerson, E., Auclair, D., Li, L., Place, C., et al. (2012). A landscape of driver mutations in melanoma. Cell *150*, 251–263.

Horn, S., Figl, A., Rachakonda, P.S., Fischer, C., Sucker, A., Gast, A., Kadel, S., Moll, I., Nagore, E., Hemminki, K., et al. (2013). TERT promoter mutations in familial and sporadic melanoma. Science *339*, 959–961.

Huang, F.W., Hodis, E., Xu, M.J., Kryukov, G.V., Chin, L., and Garraway, L.A. (2013). Highly recurrent TERT promoter mutations in human melanoma. Science *339*, 957–959.

Jayaraman, S.S., Rayhan, D.J., Hazany, S., and Kolodney, M.S. (2014). Mutational landscape of basal cell carcinomas by whole-exome sequencing. J. Invest. Dermatol. *134*, 213–220.

Ji, Z., Kumar, R., Taylor, M., Rajadurai, A., Marzuka-Alcalá, A., Chen, Y.E., Njauw, C.N., Flaherty, K., Jönsson, G., and Tsao, H. (2013). Vemurafenib synergizes with nutlin-3 to deplete survivin and suppresses melanoma viability and tumor growth. Clin. Cancer Res. *19*, 4383–4391.

Kirkwood, J.M., Strawderman, M.H., Ernstoff, M.S., Smith, T.J., Borden, E.C., and Blum, R.H. (1996). Interferon alfa-2b adjuvant therapy of high-risk resected cutaneous melanoma: the Eastern Cooperative Oncology Group Trial EST 1684. J. Clin. Oncol. *14*, 7–17.

Krauthammer, M., Kong, Y., Ha, B.H., Evans, P., Bacchiocchi, A., McCusker, J.P., Cheng, E., Davis, M.J., Goh, G., Choi, M., et al. (2012). Exome sequencing identifies recurrent somatic RAC1 mutations in melanoma. Nat. Genet. *44*, 1006–1014.

Küsters-Vandevelde, H.V., Klaasen, A., Küsters, B., Groenen, P.J., van Engen-van Grunsven, I.A., van Dijk, M.R., Reifenberger, G., Wesseling, P., and Blokx, W.A. (2010). Activating mutations of the GNAQ gene: a frequent event in primary melanocytic neoplasms of the central nervous system. Acta Neuropathol. *119*, 317–323.

Lawrence, M.S., Stojanov, P., Polak, P., Kryukov, G.V., Cibulskis, K., Sivachenko, A., Carter, S.L., Stewart, C., Mermel, C.H., Roberts, S.A., et al. (2013). Mutational heterogeneity in cancer and the search for new cancer-associated genes. Nature *499*, 214–218.

Lawrence, M.S., Stojanov, P., Mermel, C.H., Robinson, J.T., Garraway, L.A., Golub, T.R., Meyerson, M., Gabriel, S.B., Lander, E.S., and Getz, G. (2014). Discovery and saturation analysis of cancer genes across 21 tumour types. Nature *505*, 495–501.

Lopez, G.Y., Reitman, Z.J., Solomon, D., Waldman, T., Bigner, D.D., McLendon, R.E., Rosenberg, S.A., Samuels, Y., and Yan, H. (2010). IDH1(R132) mutation identified in one human melanoma metastasis, but not correlated with metastases to the brain. Biochem. Biophys. Res. Commun. *398*, 585–587.

Lutzky, J., Bauer, J., and Bastian, B.C. (2008). Dose-dependent, complete response to imatinib of a metastatic mucosal melanoma with a K642E KIT mutation. Pigment Cell Melanoma Res. *21*, 492–493.

Maertens, O., Johnson, B., Hollstein, P., Frederick, D.T., Cooper, Z.A., Messiaen, L., Bronson, R.T., McMahon, M., Granter, S., Flaherty, K., et al. (2013). Elucidating distinct roles for NF1 in melanomagenesis. Cancer Discov. *3*, 338–349.

Mann, G.J., Pupo, G.M., Campain, A.E., Carter, C.D., Schramm, S.J., Pianova, S., Gerega, S.K., De Silva, C., Lai, K., Wilmott, J.S., et al. (2013). BRAF mutation, NRAS mutation, and the absence of an immune-related expressed gene profile predict poor outcome in patients with stage III melanoma. J. Invest. Dermatol. *133*, 509–517.

McArthur, G.A., and Ribas, A. (2013). Targeting oncogenic drivers and the immune system in melanoma. J. Clin. Oncol. *31*, 499–506.

Mihm, M.C., Jr., Clemente, C.G., and Cascinelli, N. (1996). Tumor infiltrating lymphocytes in lymph node melanoma metastases: a histopathologic prognostic indicator and an expression of local immune response. Lab. Invest. *74*, 43–47.

Morton, D.L., Thompson, J.F., Cochran, A.J., Mozzillo, N., Nieweg, O.E., Roses, D.F., Hoekstra, H.J., Karakousis, C.P., Puleo, C.A., Coventry, B.J., et al.; MSLT Group (2014). Final trial report of sentinel-node biopsy versus nodal observation in melanoma. N. Engl. J. Med. *370*, 599–609.

Nikolaev, S.I., Rimoldi, D., Iseli, C., Valsesia, A., Robyr, D., Gehrig, C., Harshman, K., Guipponi, M., Bukach, O., Zoete, V., et al. (2012). Exome sequencing identifies recurrent somatic MAP2K1 and MAP2K2 mutations in melanoma. Nat. Genet. *44*, 133–139.

Nissan, M.H., Pratilas, C.A., Jones, A.M., Ramirez, R., Won, H., Liu, C., Tiwari, S., Kong, L., Hanrahan, A.J., Yao, Z., et al. (2014). Loss of NF1 in cutaneous melanoma is associated with RAS activation and MEK dependence. Cancer Res. *74*, 2340–2350.

Noushmehr, H., Weisenberger, D.J., Diefes, K., Phillips, H.S., Pujara, K., Berman, B.P., Pan, F., Pelloski, C.E., Sulman, E.P., Bhat, K.P., et al.; Cancer Genome Atlas Research Network (2010). Identification of a CpG island methylator phenotype that defines a distinct subgroup of glioma. Cancer Cell *17*, 510–522.

Pollock, P.M., Harper, U.L., Hansen, K.S., Yudt, L.M., Stark, M., Robbins, C.M., Moses, T.Y., Hostetter, G., Wagner, U., Kakareka, J., et al. (2003). High frequency of BRAF mutations in nevi. Nat. Genet. *33*, 19–20.

Rakosy, Z., Ecsedi, S., Toth, R., Vizkeleti, L., Hernandez-Vargas, H., Lazar, V., Emri, G., Szatmari, I., Herceg, Z., Adany, R., and Balazs, M. (2013). Integrative genomics identifies gene signature associated with melanoma ulceration. PLoS ONE *8*, e54958.

Ranzani, M., Alifrangis, C., Perna, D., Dutton-Regester, K., Pritchard, A., Wong, K., Rashid, M., Robles-Espinoza, C.D., Hayward, N.K., McDermott, U., et al. (2015). BRAF/NRAS wild-type melanoma, NF1 status and sensitivity to trametinib. Pigment Cell Melanoma Res. *28*, 117–119.

Robbins, P.F., Lu, Y.C., El-Gamil, M., Li, Y.F., Gross, C., Gartner, J., Lin, J.C., Teer, J.K., Cliften, P., Tycksen, E., et al. (2013). Mining exomic sequencing data to identify mutated antigens recognized by adoptively transferred tumor-reactive T cells. Nat. Med. *19*, 747–752.

Robert, C., Ribas, A., Wolchok, J.D., Hodi, F.S., Hamid, O., Kefford, R., Weber, J.S., Joshua, A.M., Hwu, W.J., Gangadhar, T.C., et al. (2014). Anti-programmed-death-receptor-1 treatment with pembrolizumab in ipilimumab-refractory advanced melanoma: a randomised dose-comparison cohort of a phase 1 trial. Lancet *384*, 1109–1117.

Santa Cruz, D.J., Hamilton, P.D., Klos, D.J., and Fernandez-Pol, J.A. (1997). Differential expression of metallopanstimulin/S27 ribosomal protein in melanocytic lesions of the skin. J. Cutan. Pathol. *24*, 533–542.

Shields, J.M., Thomas, N.E., Cregger, M., Berger, A.J., Leslie, M., Torrice, C., Hao, H., Penland, S., Arbiser, J., Scott, G., et al. (2007). Lack of extracellular signal-regulated kinase mitogen-activated protein kinase signaling shows a new type of melanoma. Cancer Res. *67*, 1502–1512.

Snyder, A., Makarov, V., Merghoub, T., Yuan, J., Zaretsky, J.M., Desrichard, A., Walsh, L.A., Postow, M.A., Wong, P., Ho, T.S., et al. (2014). Genetic basis for clinical response to CTLA-4 blockade in melanoma. N. Engl. J. Med. *371*, 2189–2199.

Sun, D., Li, Z., Rew, Y., Gribble, M., Bartberger, M.D., Beck, H.P., Canon, J., Chen, A., Chen, X., Chow, D., et al. (2014). Discovery of AMG 232, a potent, selective, and orally bioavailable MDM2-p53 inhibitor in clinical development. J. Med. Chem. *57*, 1454–1472.

TCGA (Cancer Genome Atlas Research Network) (2008). Comprehensive genomic characterization defines human glioblastoma genes and core pathways. Nature *455*, 1061–1068.

TCGA (Cancer Genome Atlas Research Network) (2012). Comprehensive genomic characterization of squamous cell lung cancers. Nature *489*, 519–525.

TCGA (Cancer Genome Atlas Research Network) (2014a). Comprehensive molecular characterization of urothelial bladder carcinoma. Nature *507*, 315–322.

TCGA (Cancer Genome Atlas Research Network) (2014b). Comprehensive molecular profiling of lung adenocarcinoma. Nature *511*, 543–550.

Terheyden, P., Houben, R., Pajouh, P., Thorns, C., Zillikens, D., and Becker, J.C. (2010). Response to imatinib mesylate depends on the presence of the V559A-mutated KIT oncogene. J. Invest. Dermatol. *130*, 314–316.

Topalian, S.L., Hodi, F.S., Brahmer, J.R., Gettinger, S.N., Smith, D.C., McDermott, D.F., Powderly, J.D., Carvajal, R.D., Sosman, J.A., Atkins, M.B., et al. (2012). Safety, activity, and immune correlates of anti-PD-1 antibody in cancer. N. Engl. J. Med. *366*, 2443–2454.

Tsao, H., Chin, L., Garraway, L.A., and Fisher, D.E. (2012). Melanoma: from mutations to medicine. Genes Dev. *26*, 1131–1155.

Tumeh, P.C., Harview, C.L., Yearley, J.H., Shintaku, I.P., Taylor, E.J., Robert, L., Chmielowski, B., Spasic, M., Henry, G., Ciobanu, V., et al. (2014). PD-1 blockade induces responses by inhibiting adaptive immune resistance. Nature 515, 568–571.

Van Allen, E.M., Wagle, N., Sucker, A., Treacy, D.J., Johannessen, C.M., Goetz, E.M., Place, C.S., Taylor-Weiner, A., Whittaker, S., Kryukov, G.V., et al.; Dermatologic Cooperative Oncology Group of Germany (DeCOG) (2014). The genetic landscape of clinical resistance to RAF inhibition in metastatic melanoma. Cancer Discov. 4, 94–109.

Watson, I.R., Li, L., Cabeceiras, P.K., Mahdavi, M., Gutschner, T., Genovese, G., Wang, G., Fang, Z., Tepper, J.M., Stemke-Hale, K., et al. (2014). The RAC1 P29S hotspot mutation in melanoma confers resistance to pharmacological inhibition of RAF. Cancer Res. 74, 4845–4852.

Whittaker, S.R., Theurillat, J.P., Van Allen, E., Wagle, N., Hsiao, J., Cowley, G.S., Schadendorf, D., Root, D.E., and Garraway, L.A. (2013). A genome-scale RNA interference screen implicates NF1 loss in resistance to RAF inhibition. Cancer Discov. 3, 350–362.

Winnepenninckx, V., Lazar, V., Michiels, S., Dessen, P., Stas, M., Alonso, S.R., Avril, M.F., Ortiz Romero, P.L., Robert, T., Balacescu, O., et al.; Melanoma Group of the European Organization for Research and Treatment of Cancer (2006). Gene expression profiling of primary cutaneous melanoma and clinical outcome. J. Natl. Cancer Inst. 98, 472–482.